Biomedicine & Pharmacotherapy 188 (2025) 118181

Contents lists available at ScienceDirect

Biomedicine & Pharmacotherapy

journal homepage: www.elsevier.com/locate/biopha

Notoginsenoside Ft1 induces lysosomal cell death and apoptosis by inhibiting the PI3K/AKT/mTOR pathway in hepatocellular carcinoma

Youngsic Jeon [a], Hyukjoon Kwon [a], Taek Chung [b], Young Nyun Park [c], Su-Nam Kim [a,d], Jun Yeon Park [e], Ki Sung Kang [f], Dong-Young Woo [d], Taejung Kim [a,d,*], Young-Joo Kim [a,**]

[a] Institute of Natural Products, Korea Institute of Science and Technology, Republic of Korea
[b] Department of Pathology, Yonsei University College of Medicine, Republic of Korea
[c] Department of Pathology, Graduate School of Medical Science, Brain Korea 21 Project, Yonsei University College of Medicine, Republic of Korea
[d] Natural Product Applied Science, KIST School, University of Science and Technology, Republic of Korea
[e] Vital To Life Co., Ltd., Republic of Korea
[f] College of Korean Medicine, Gachon University, Republic of Korea

ARTICLE INFO

Keywords:
Apoptosis
Lysosomal cell death
Notoginsenoside Ft1
PI3K/AKT/mTOR pathway
TFEB

ABSTRACT

Notoginsenoside Ft1 (NFt1) is a bioactive compound derived from *Panax notoginseng*, a traditional medicinal herb that exhibits various pharmacological properties, including anti-inflammatory and anticancer effects. However, its effects on hepatocellular carcinoma (HCC) remain poorly understood. This study sought to investigate the anticancer effects of NFt1 and uncover its fundamental mechanisms in HCC cells. NFt1 treatment inhibited cell proliferation and promoted apoptosis by enhancing cell death markers. Transcriptome profiling using RNA-sequencing revealed that NFt1 treatment downregulated the expression of oncogenes (e.g., *FOS*, *BRAF*, *RARA*, *MYC*, and *JUND*), while upregulating lysosomal cell death-related genes (e.g., *CTSB*, *CTSD*, *LAMP1*, *LAMP2*, and *TPP1*). These effects are associated with PI3K/AKT/mTOR inhibition and increased transcriptional activity of transcription factor EB (TFEB). NFt1 treatment induced autophagic traits by suppressing the PI3K/AKT/mTOR pathway, thereby enhancing TFEB transactivity. These findings demonstrated the therapeutic promise of NFt1 in the effective management of HCC.

1. Introduction

Hepatocellular carcinoma (HCC) continues to be a major mortality to global cancer-related death, with scarce therapeutic options and a poor prognosis in advanced stages [1,2]. Despite recent advances in therapeutic strategies, there is a need for more effective and targeted approaches [3]. Natural products derived from traditional medicinal herbs have garnered significant attention owing to their diverse pharmacological properties and potential for use as anticancer agents.

Panax notoginseng, a traditional medicinal herb, has been extensively studied for its therapeutic properties, including anti-inflammatory, cardiovascular protective, and anticancer effects [4–6]. Notoginsenoside Ft1 (NFt1) has emerged as a promising bioactive compound with a broad range of biological activities. While NFt1 has shown notable efficacy in various cancer models, its effects on HCC remain largely unexplored.

The PI3K/AKT/mTOR pathway is a critical regulator of cell survival, proliferation, and metabolism and is often dysregulated in HCC [7]. Additionally, growing evidence has highlighted the critical role of lysosome-mediated cell death as a complementary mechanism for overcoming resistance to conventional therapies [8,9]. Lysosomes, which are essential for cellular homeostasis, play a key role in degrading damaged organelles and proteins, and their dysregulation is frequently implicated in cancer progression.

Transcription factor EB (TFEB) is a key mediator of lysosomal function and cell death under stress conditions. Its phosphorylation and activation by the AKT/mTOR signaling pathway play a critical role in promoting lysosomal biogenesis and autophagy. Notably, modulation of AKT activity influences TFEB phosphorylation and nuclear translocation, thereby suppressing lysosomal gene expression and traits [10,11]. The ability of therapeutic agents to modulate lysosomal activity offers a unique approach for targeting cancer cells [9,12,13].

* Corresponding author at: Institute of Natural Products, Korea Institute of Science and Technology, Republic of Korea.
** Corresponding author.
E-mail addresses: kgsing@kist.re.kr (T. Kim), yjkim7801@kist.re.kr (Y.-J. Kim).

https://doi.org/10.1016/j.biopha.2025.118181
Received 23 March 2025; Received in revised form 13 May 2025; Accepted 21 May 2025
Available online 31 May 2025

In this study, we investigate the anticancer properties of NFt1 in HCC and elucidated the molecular pathways involved. By integrating *in vitro* and *in vivo* approaches, along with transcriptomic analysis, we aimed to uncover the therapeutic potential of NFt1 and its role in modulating lysosomal-mediated cell death and autophagic processes. Our findings offer new perspectives on the anticancer properties of NFt1 and its promise as an innovative treatment agent for HCC.

2. Materials and methods

2.1. Chemicals and xenograft mouse model

Information on Notoginsenoside Ft1 (NFt1) and the 36 other ginsenosides used in this study is provided in Table S1. Balb/C Nube mice (5 weeks old) were purchased from Orient Bio (Seongnam, Korea). To establish the xenograft mouse model, HepG2 cells (1×10^7 cells/ 100 μL) suspended in RPMI medium (Gibco, Carlsbad, CA, USA) were implanted into the right rear dorsal flank of each mouse. Mice with tumors larger than 100 mm^3 were selected and divided into three groups: (1) untreated group (mock), which received the vehicle; (2) NFt1-treated group, which received NFt1 at 25 mg/kg every day; and (3) NFt1-treated group, which received NFt1 at 50 mg/kg every day. During the 3-week observation period, individual body weights were recorded, and the mice were monitored every 2 days for abnormal behavior, symptoms, and mortality. Approval for all procedures was granted by KIST's Institutional Animal Care and Use Committee (approval no. KIST-IACUC-2024–034) and followed established guidelines.

2.2. Histological and apoptotic analysis

The tissue sections for H&E staining were fixed in formalin (Thermo Fisher Scientific, San Jose, CA, USA), paraffin-embedded, and then deparaffinized and rehydrated. The sections were then stained with 85 % hematoxylin (Thermo Fisher Scientific) to visualize the nuclei and eosin Y (Thermo Fisher Scientific) to highlight cytoplasmic components.

A TUNEL assay was performed to identify apoptotic cells in tumor tissues, utilizing an in situ Apoptosis Detection Kit (Takara Bio Inc., Kusatsu, Shiga, Japan). After rehydration and deparaffinization, the tissue sections were permeabilized with proteinase K (Thermo Fisher Scientific) to enhance permeability and incubated with the TdT enzyme kit to label fragmented DNA, as per the manufacturer's guidelines.

2.3. Cell maintenance

HepG2 and THLE-2 cells were obtained from the American Type Culture Collection (ATCC, Manassas, VA, USA) and Huh7 and PCL/PRF/5 cells were obtained from the Korean Cell Line Bank (Seoul, Korea). HepG2 cells were cultured in MEM supplemented with 10 % fetal bovine serum (FBS; Gibco) and 1 % penicillin-streptomycin (P/S; Gibco). Hep3B and Huh7 cells were cultured in RPMI medium supplemented with 10 % FBS and 1 % P/S. THLE-2 cells were cultured in BEGM supplemented with the BEGM SingleQuots™ Kit, 10 % FBS, and 1 % P/S. All the cells were maintained at 37 °C in a humidified atmosphere containing 5 % carbon dioxide.

2.4. Cell viability assay

Cell viability was assessed using the WST-8 assay as previously described [14].

2.5. Colony formation assay

To assess the impact of NFt1 on colony formation, cells were treated with 12.5, 25, and 50 μM concentration of NFt1. The medium was replaced every three days, and after 21 days, the cells were fixed with 4 % paraformaldehyde (Thermo Fisher Scientific) and subsequently stained using a crystal violet solution. Colony formation was observed under a microscope and quantified using a Multiskan Sky microplate reader (Thermo Fisher Scientific).

2.6. Western blotting

Protein expression and phosphorylation levels were evaluated by western blotting. HCC cells were lysed in RIPA buffer (Cell Signaling Technology, Danvers, MA, USA) containing a Protease Inhibitor Cocktail (Cell Signaling Technology) and Phosphatase Inhibitor Cocktail (Cell Signaling Technology) on ice for 30 min. The cell lysates were clarified by centrifugation at 14,000 rpm and 4 °C for 15 min, and the supernatants were collected. Protein (30 – 50 μg/line) were separated by electrophoresis on NuPAGE 4–12 % Bis–Tris gels (Invitrogen, Carlsbad, CA, USA), transferred onto PVDF membranes, and analyzed using specific primary and secondary antibodies. The bound antibodies were visualized using SuperSignal™ West Femto (Thermo Fisher Scientific) and imaged using an LAS 4000 system (Fujifilm, Japan). Table S2 summarizes the details of the antibodies applied and the experimental conditions.

2.7. Flow cytometry analysis

To detect apoptotic cells, HepG2 and Huh7 cells were plated at a density of 3×10^5 cells/well in 6-well plates and incubated for 24 h. The cells were subsequently exposed to a serial dilution of NFt1. Following 24 h of treatment, cells were assessed by flow cytometry using the FITC Annexin V Apoptosis Detection Kit (BD Biosciences, Franklin Lakes, NJ, USA). Apoptotic cells were assessed by FACSVerse™ (BD Biosciences), and the results were performed using FlowJo software (TreeStar, Woodburn, OR, USA). At least 1000 cells were analyzed for each sample.

2.8. Transcriptome profiling and gene set analysis

For transcriptome profiling, HepG2 cells were plated at 3×10^5 cells/well in 6-well and incubated for 24 h. After 12 h of treatment with 50 μM NFt1, cells were harvested and RNA was extracted using an RNeasy kit (Qiagen, Hilden, Germany). FASTQ files were produced using a HiSeq 4000 (Illumina, San Diego, CA, USA). Fragments per kilobase of transcript per million mapped reads (FPKM) were calculated with TopHat and Cufflinks [15]. The obtained FPKM values were used for transcriptome profiling, carried out in R (https://www.r-project.org/). Transcriptome profiling and gene set enrichment analysis (GSEA) were carried out as previously described [16].

Gene set analysis was carried out with STRING (https://string-db.org/) using KEGG and REAC databases. GSEA was performed using the KEGG (http://www.genome.jp/kegg/) and Reactome (http://www.reactome.org/) databases. The list of oncogenes (n = 674) and tumor suppressor genes (TSGs, n = 1088) lists was sourced from previous studies [17,18]. The details of the data and associated references are summarized in Table S3.

2.9. Evaluation of cathepsin B and D activity

To measure cathepsin B and D activity, cell and tissue extracts (100–200 μg per reaction) were analyzed using the Cathepsin B/D Activity Assay Kit (Abcam, Cambridge, UK). Cathepsin B and D activity in the extracts was quantified using a VarioskanTM (Thermo Fisher Scientific), with filters set at 400/505 nm for cathepsin B and 328/460 nm for cathepsin D.

2.10. Assessment of TFEB transactivity

To evaluate transcription factor EB (TFEB) transactivity, a 4xTFEB-luciferase construct containing TFEB binding motifs derived from the *LAMP1* gene promoter sequences (-214 to −115 bp) was generated using

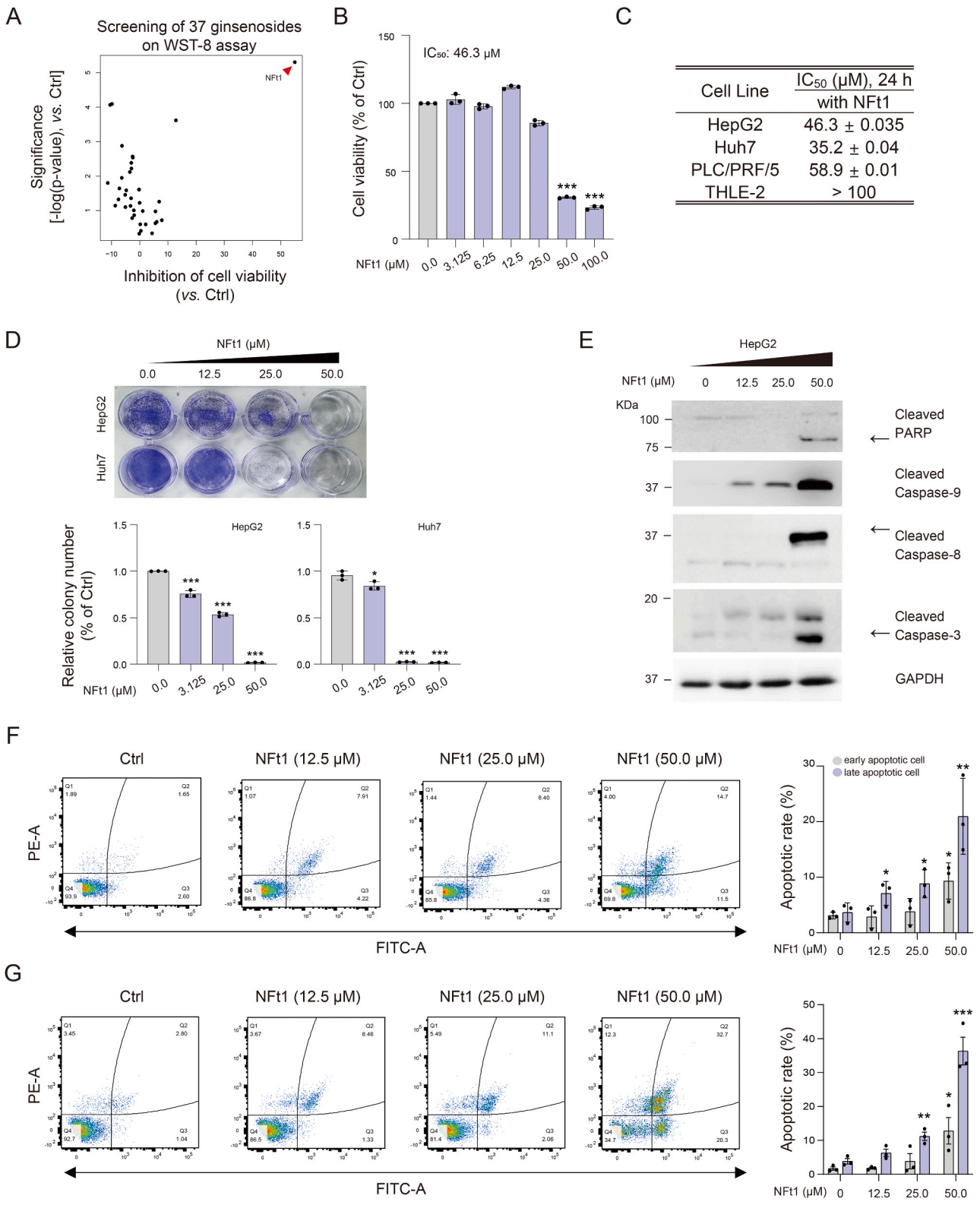

Fig. 1. Effects of notoginsenoside Ft1 on HCC cell lines. (A) The point plot shows the effect of 37 ginsenosides on cell viability in HepG2 cells, with significant p-value and inhibitory rates compared to untreated control cells (Ctrl). (B) The barplot shows cell viability following treatment (0, 6.25, 12.5, 25.0, 50.0, and 100 μM of NFt1) for 24 h, with significant p-value (*vs.* Ctrl, ***$P < 0.001$). (C) The table presents the IC_{50} values of NFt1 in various cell lines for 24 h. (D) The results of the colony formation assay are shown (*top*). The barplots show the relative colony number in NFt1-treated HepG2 and Huh7 cells after 2 weeks, with significant p-value (*vs.* Ctrl, *$P < 0.05$ and ***$P < 0.001$) (*bottom*). (E) Western blot analysis of cleaved PARP, caspase-9, caspase-8, and caspase-3 in HepG2 cells treated with NFt1 for 24 h. (F, G) Flow cytometry analysis was conducted to evaluate early apoptosis in HepG2 and Huh7 cells after incubation under specified condition for 24 h. Early and late-stage apoptotic cells were identified by the increased fluorescence intensity of FITC-labeled annexin V (*left*). The barplot indicates the mean ± SD ($n = 3$ per group), with significant *P*-value (*vs.* Ctrl, *$P < 0.05$ and ***$P < 0.001$) (*right*).

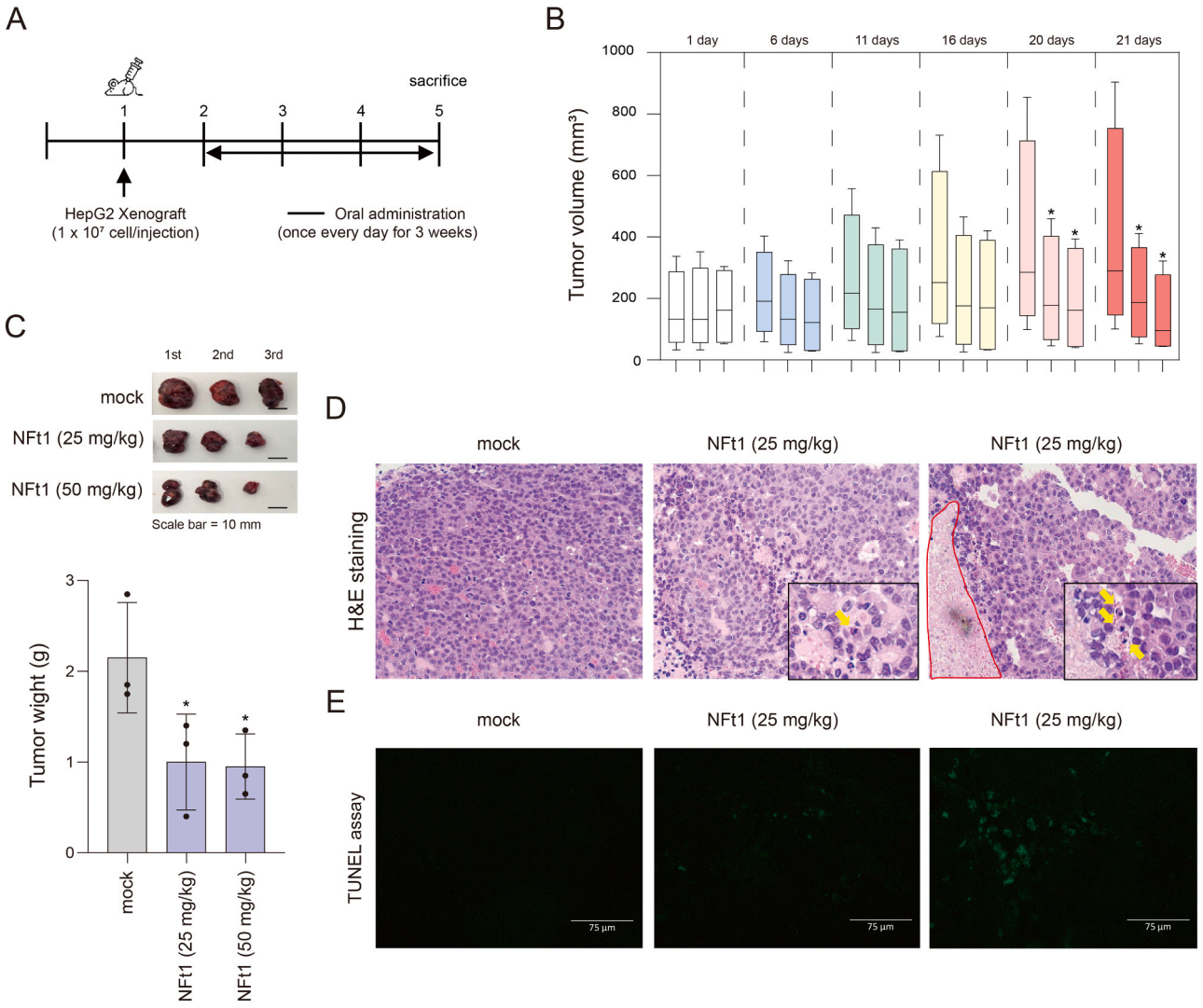

Fig. 2. Effects of notoginsenoside Ft1 on HepG2 xenograft *in vivo* model. (A) A schematic illustrating the comprehensive schedule of the HepG2 xenograft experiment. (B) Box plot indicates tumor volume in xenograft mice over the experimental period. (C) Images of dissected tumors from each group are shown as representatives (*top*). The boxplot indicates tumor weight on the final day of sacrifice, with significant *P*-value (*vs.* mock, $*P < 0.05$) (*bottom*). (D, E) Histological analysis of xenograft tissues using H&E staining (x200 and x400) and TUNEL (x200) assay; yellow arrows indicate the apoptotic cells (nuclear pyknosis and karyorrhexis), and the red line marks areas of necrosis.

the pGL3.0-basic vector (Promega, Madison, WI, USA). HepG2 cells were seeded in 96-well plates (SPL Life Science, Pocheon, Korea) and incubated for 24 h. Transfection was performed using 125 ng of the reporter construct and 0.25 ng of the pNL1.1.TK vector per well with 0.5 μl FuGENE® HD Transfection Reagent (Promega).

Following 24 h of transfection, cells were treated with NFt1 at 12.5, 25, and 50 μM. After 24 h of treatment, luciferase activity was quantified using the Nano-Glo® Dual Luciferase® Reporter Assay System (Promega), with firefly luciferase normalized to NanoLuc™ to adjust for transfection efficiency. Details of primer sequences and thermal cycling parameters are provided in Table S4.

2.11. Data analysis

The plots show mean values ± standard deviation (S.D.) from at least three independent experiments. Transcriptome profiling was analyzed using the R programming language, while experimental data were processed and analyzed with GraphPad Prism 6. Statistical significance was determined by the Student's *t*-test, with $P < 0.05$ considered significant.

3. Results

3.1. Effects of notoginsenoside Ft1 on HCC cell lines

Initially, we performed a preliminary screening of various ginsenosides ($n = 37$, Table S1 and Fig. S1) and identified notoginsenoside Ft1 (NFt1) as a potent compound, exhibiting a stronger inhibitory effect on cell viability than other ginsenosides (55.0 %, Fig. 1A). We then assessed the viability of other HCC cell lines and a normal hepatic cell line (e.g., THLE-2) following NFt-1 treatment. Our results showed that NFt1 had inhibitory effects on HepG2 ($IC_{50} = 46.3$ μM), Huh7 ($IC_{50} = 35.2$ μM), and PLC/PRF/5 ($IC_{50} = 58.9$ μM) cells, but not on THLE-2 ($IC_{50} = 82.2$ μM) cells (Fig. 1B, C, and Fig. S2). Based on these findings, HepG2 and Huh7 cells were selected for further experiments because of their demonstrated snesitivity to NFt1's anticancer effects. Additionally, NFt1 treatment at different concentration (12.5, 25.0, and 50.0 μM) significantly suppressed tumor colony formation in HCC cells (Fig. 1D) and increased the expression of apoptotic proteins including poly (ADP-ribose) polymerase, casepase-9, caspase-8, and caspase-3 (Fig. 1E and Fig. S3). To further investigate the apoptotic response induced by NFt1 treatment, fluorescence-activated cell sorting analysis was conducted,

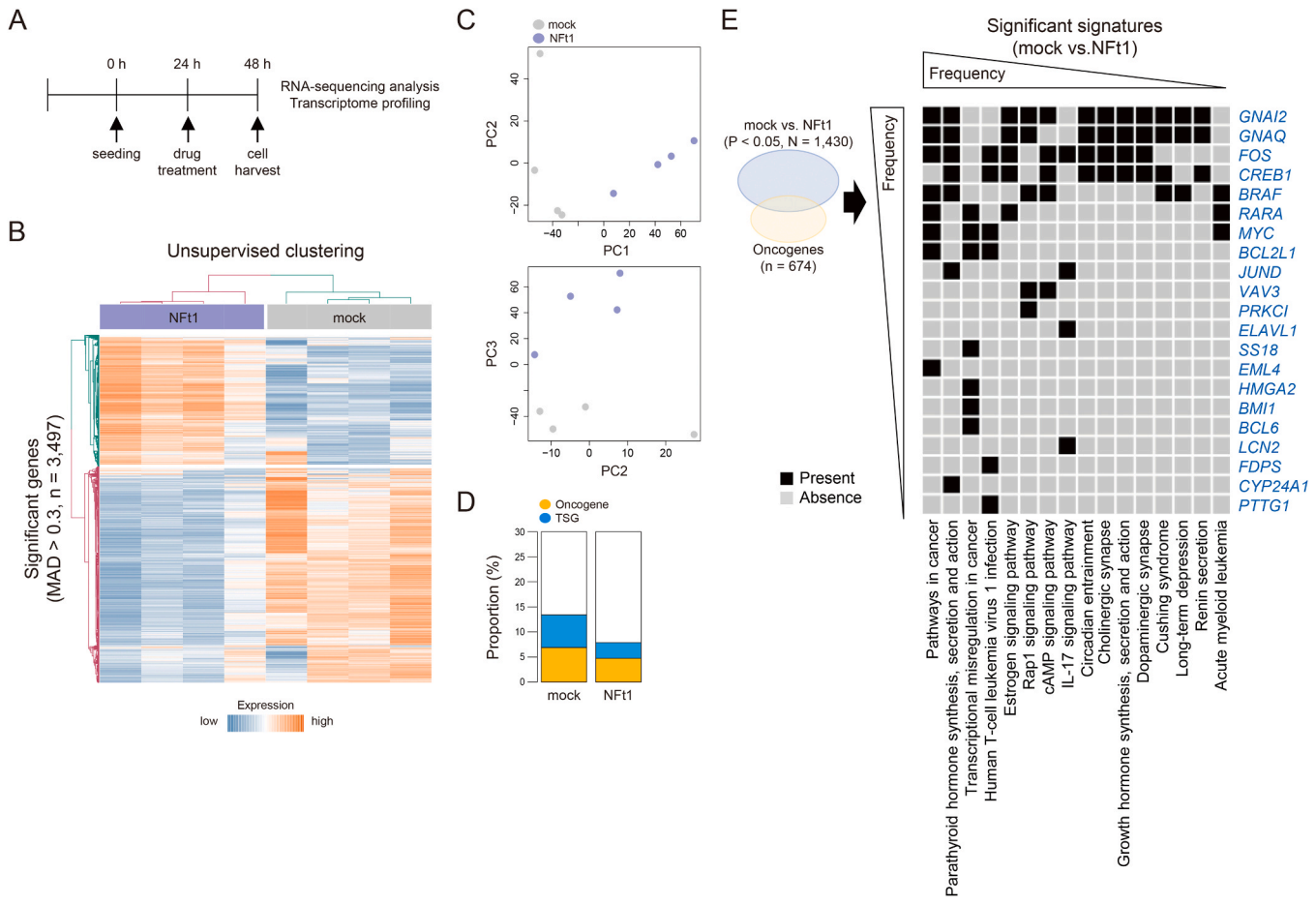

Fig. 3. Transcriptomic profiling of notoginsenoside Ft1 on HepG2 cell line. (A) A schematic representation of the sampling process for RNA-seq of NFt1 treated HepG2 cells. For further details, refer to the Materials and Methods. (B) A heatmap showing unsupervised clustering based on genes with variable expression (MAD > 0.3, $n = 6916$). (C) PCA of variably expressed genes (MAD > 0.3, $n = 3497$) highlights the distinct distribution between untreated control cells (mock) and NFt1-treated cells. (D) Boxplot shows the proportion of oncogenes and tumor suppressor genes in each group. (E) The heatmap shows significantly differentially expressed genes (mock *vs.* NFt1, $P < 0.05$, $n = 1430$), including oncogenes ($n = 674$) and their associated KEGG pathway signatures across the groups.

revealing a marked rise in both early and late apoptotic HepG2 and Huh7 cells (Fig. 1F and G).

3.2. Effects of notoginsenoside Ft1 on HepG2 Xenograft in vivo model

To investigate the *in vivo* effects of NFt1, a HepG2 xenograft model was generated and administered a selected dose of NFt1 (Fig. 2A). These concentrations were selected based on preliminary results showing no significant impact on body weight in mice (Fig. S4). The effects of NFt1 treatment on tumor size were evaluated in a HepG2 xenograft model. NFt1 treatment led to a significant reduction in tumor size compared to untreated mice (mock) on 20 and 21 days ($P < 0.05$, Fig. 2B). While the tumor weight between the two NFt1 concentrations (25 and 50 mg/kg) showed no notable variation, a reduction in tumor weight was observed with NFt1 treatment relative to the mock group ($P < 0.05$, Fig. 2C). Additionally, we validated our findings using histological analysis and TUNEL assay to detect apoptotic cells in HepG2 xenograft mouse tissues. NFt1 treatment exhibited histological features of apoptosis, including pyknotic changes in nuclei and karyorrhexis, compared to the mock group (Fig. 2D). Furthermore, NFt1 treatment led to a marked increase in apoptotic cells compared to the mock group (Fig. 2E). Taken together, NFt1 treatment reduced tumor size while increasing pyknosis and apoptosis, confirming its anti-cancer effects.

3.3. Transcriptomic profiling of notoginsenoside Ft1 on HCC cell line

To elucidate the fundamental mechanisms of NFt1 in HCC cell lines, we performed RNA-sequencing (RNA-seq) to analyze the transcriptomic profile (Fig. 3A). Unsupervised clustering of highly variable genes (MAD > 0.5, $n = 6916$) showed distinct transcriptomic separation between NFt1-treated and untreated cells, clearly reflecting their treatment status (Fig. 3B). Additionally, principal component analysis revealed that NF1-treated and untreated cells clustered separately, indicating distinct transcriptomic traits (Fig. 3C). Upon analyzing the proportion of oncogenes and TSGs between these groups, we observed a significant change in the proportion of oncogenes, but not in TSGs (Fig. 3D). Furthermore, NFt1-treated cells exhibited reduced expression of cancer-related signatures linked to oncogenes (e.g., pathways in cancer, parathyroid hormone synthesis, secretion and action, transcriptional misregulation in cancer). Among these oncogenes, *FOS*, *BRAF*, *RARA*, *MYC*, and *JUND*, which are highly relevant to HCC pathogenesis, exhibited notable variations between the groups ($P < 0.05$, Fig. 3E).

3.4. Notoginsenoside Ft1 inhibits the AP-1 activation via suppressing KRAS, FOS and JUND expression

To identify robust genes regardless of group, we analyzed the differentially expressed genes (DEGs), categorizing them as NFt1 signature "Up genes" ($n = 563$) and "Down genes" ($n = 869$) ($P < 0.05$, fold change [FC] > 0.5; Fig. 4A and Table S2). The "Down genes" were

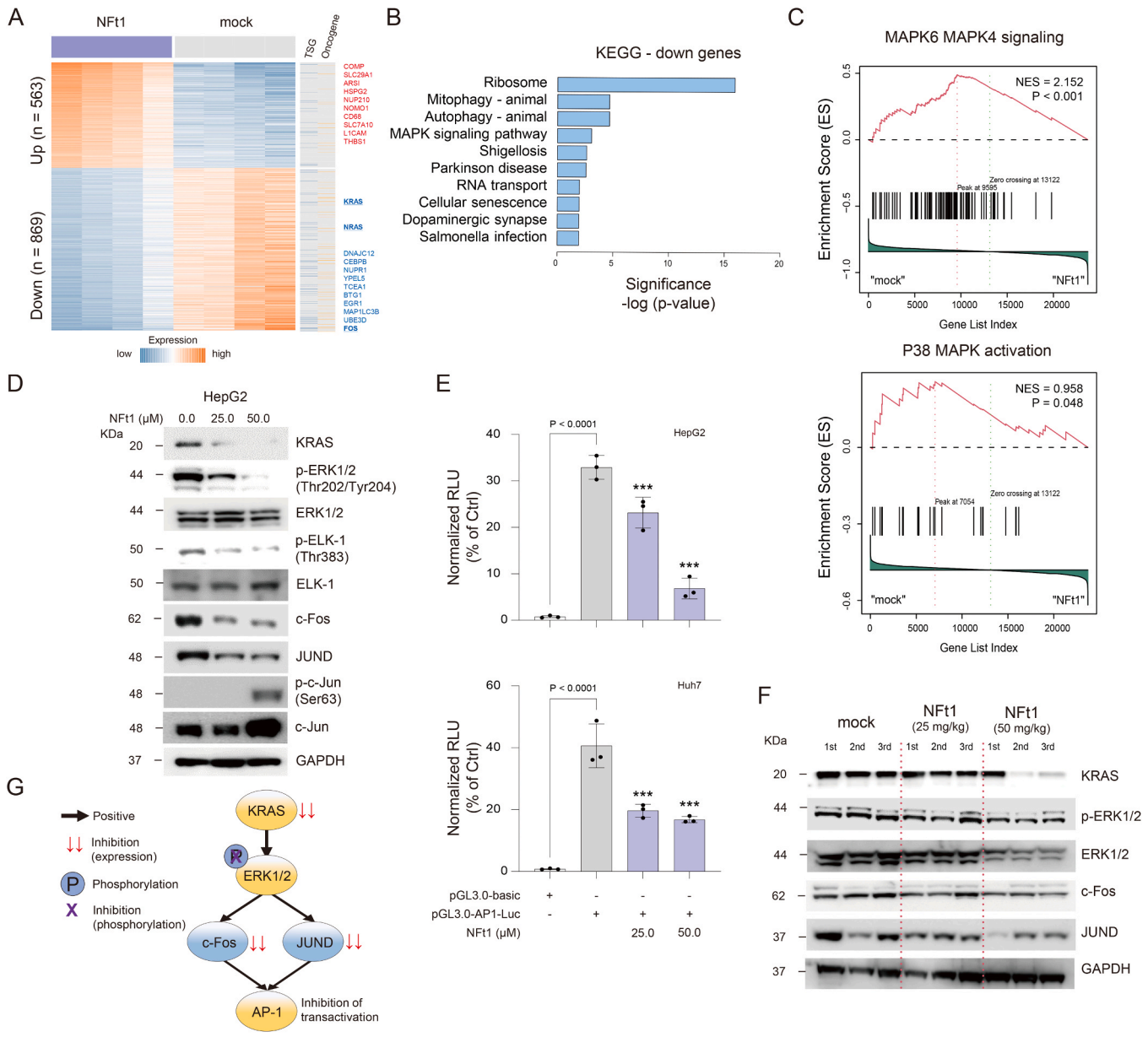

Fig. 4. Notoginsenoside Ft1 inhibits the AP-1 activation via suppressing KRAS, FOS and JUND expression. (A) A heatmap displays the DEGs (Up genes, $n = 563$; Down genes, $n = 869$), with key oncogenes and TSGs labeled on the right. (B) The barplot shows significantly enriched down gene signatures between the mock and NFt1-treated groups, with *P*-values indicating the significance of gene sets (KEGG). (C) GSEA analysis reveals enrichment of MAPK-related signatures from the KEGG and REAC databases. (D) Western blot analysis of KRAS, phospho-ERK1/2, ERK1/2, phospho-ELK-1, ELK-1, c-Fos, JUND, phospho-c-Jun, and c-Jun in HepG2 cells treated with NFt1 for 24 h. (E) The barplot shows AP-1 transactivation in HepG2 and Huh7 cells following 24 h of NFt1 treatment, with significant p-value (vs. Ctrl; 2 line, $^{***}P < 0.001$). (F) Western blot analysis of KRAS, phospho-ERK1/2, ERK1/2, c-Fos, and JUND in HepG2 xenograft tissue untreated and treated with NFt1 (25 and 50 mg/kg). GAPDH is used as the loading control. (G) Summary of NFt1's effects on KRAS/MAPK pathway.

significantly associated with the MAPK signaling pathway, including *FOS* (FC = −2.48), *JUND* (FC = −1.19), *NRAS* (FC = −0.97), and *KRAS* (FC = −0.76) (Fig. 4B). Moreover, gene set enrichment analysis (GSEA) showed upregulation of the "MAPK6_MAPK4_signaling" and "P38_MAPK_activation" signatures (Fig. 4C), which are known to contribute to HCC pathogenesis [19]. Moreover, we observed a dose-dependent reduction in the expression of proteins such as KRAS, c-Fos, and JUND, as well as in the phosphorylation levels of extracellular signal-regulated kinase 1/2 (ERK1/2) and ETS Transcription Factor ELK1 (ELK-1) in NFt1-treated HCC cells. In contrast, the phosphorylation of c-Jun was found to increase in a dose-dependent manner (Fig. 4D and Fig. S5). Furthermore, using the AP-1 reporter assay, we confirmed that NFt1 treatment significantly suppressed AP-1 transactivity compared to untreated cells (Fig. 4E). To confirm our findings, we examined KRAS, ERK1/2, c-Fos, and JUND proteins levels in xenograft mouse tissues from different treatment groups (e.g., mock and NFt1 25 and 50 mg/kg) and observed a notable reduction in their expression (Fig. 4F). Collectively, our findings suggest that NFt1 treatment leads to the suppression of MAPK pathway-related protein expression and inhibition of its downstream signaling molecules (Fig. 4G).

3.5. *Notoginsenoside Ft1 accelerates the lysosomal cell death*

Next, we evaluated significantly enriched up gene signatures and found that lysosome-related genes emerged as a prominent category (Fig. 5A). Lysosomal traits are associated with cell death [20].

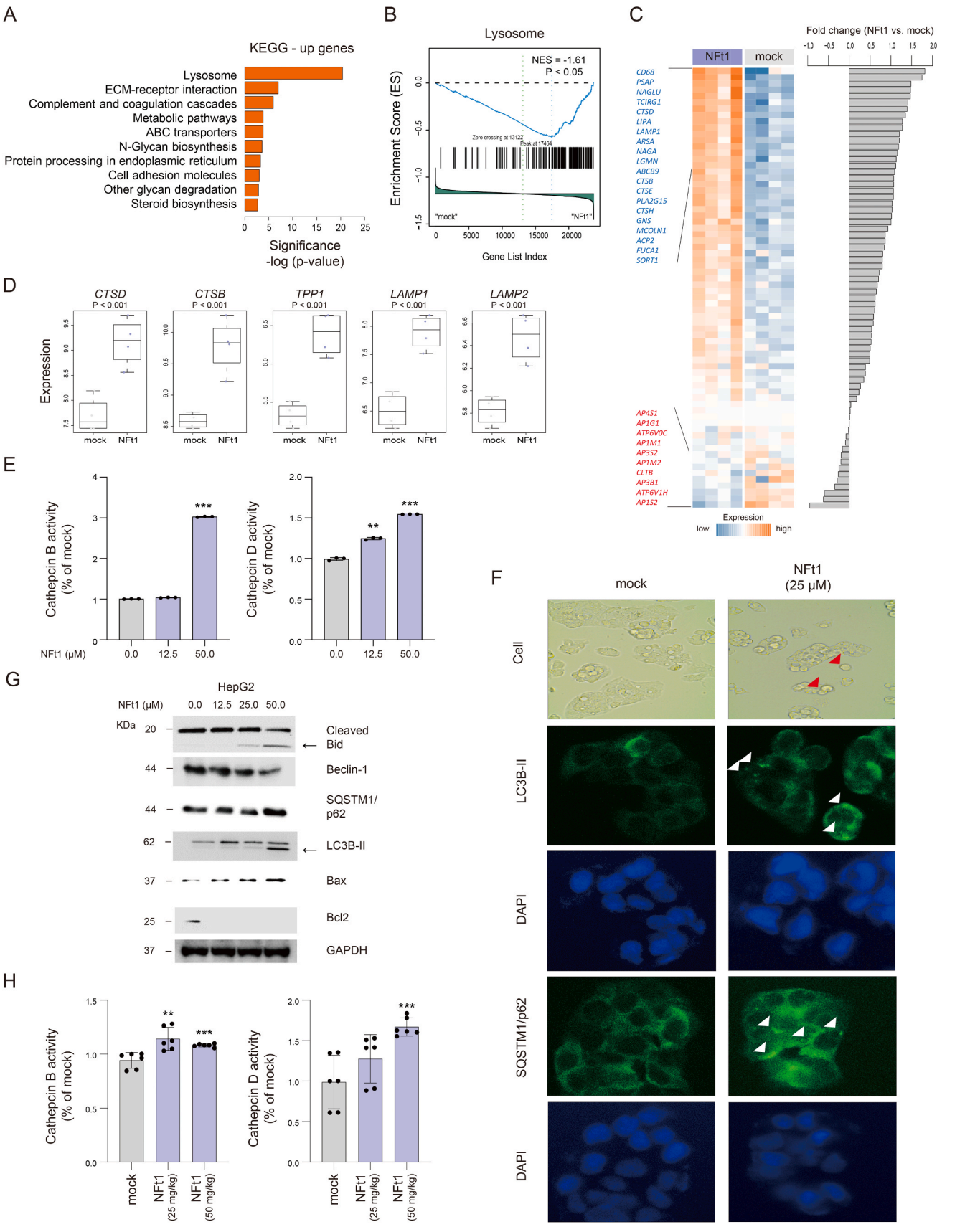

(caption on next page)

Fig. 5. Notoginsenoside Ft1 accelerates the lysosomal cell death. (A) The barplot shows significantly enriched up gene signatures between the mock and NFt1-treated groups, with p-values indicating the significance of KEGG gene sets. (B) GSEA results show the enrichment of lysosome-related signature (REAC). (C) The heatmap shows the expression levels of lysosome-related genes ($n = 70$) with fold changes between the mock and NFt1-treated groups. (D) The boxplots show the expression of lysosomal cell death-related genes, including *CTSD*, *CTSB*, *TPP1*, *LAMP1*, and *LAMP2*, with significant *P*-value. (E) The barplots show the cathepsin B and D activity in HepG2 and Huh7 cells, with significant *P*-value (*vs.* Ctrl, $^{**}P < 0.01$ and $^{***}P < 0.001$). (F) Cell morphology and confocal immunofluorescence images of LC3B (*green*), SQSTM1/p62 (*green*), and DAPI (*blue*) in HepG2 cells, untreated and treated with NFt1, were captured using the EVOS™ M5000 imaging system. (G) Western blot analysis of cleaved BiD, Becline-1, SQSTM1/p62, LC3B, Bax, and Bcl2 in HepG2 cells treated with NFt1 for 24 h. (H) The barplots show the cathepsin B and D activity in HepG2 xenograft tissues, with significant p-value (*vs.* mock, $^{**}P < 0.01$ and $^{***}P < 0.001$).

Additionally, most lysosome-related genes (n = 70) showed increased expression in NFt1-treated cells compared to untreated cells (Fig. 5B and C). Among these genes, those involved in lysosomal cell death [20,21], such as *CTSB* (FC = 1.20), *CTSD* (FC = 1.47), *TPP1* (FC = 1.06), *LAMP1* (FC = 1.39), and *LAMP2* (FC = 0.65), were significantly upregulated in NFt1-treated cells ($P < 0.05$, Fig. 5D). Specifically, capthesin B and D activity in HCC cells significantly increased following NFt1 treatment, suggesting that NFt1 enhances lysosomal cell death through cathepsin B and D activation ($P < 0.05$, Fig. 5E). We also demonstrated that NFt1-treated cells exhibited both autophagosome-related traits (e.g., LC3B-II) and cell death marker (e.g., p62) from a morphological perspective (Fig. 5F). Furthermore, lysosomal cell death markers, including cleaved BiD, SQSTM1/p62, and LC3B-II, exhibited dose-dependent increases in NFt1-treated cells, along with upregulated Bcl2 associated x (Bax) and reduced B-cell leukemia/lymphoma 2 (Bcl2) expression (Fig. 5G and Fig. S6). To validate our findings, we assessed cathepsin B and D activities in xenograft mouse tissues from various treatment groups. This analysis revealed a significant higher activity in the NFt1-treated groups relative to the mock group (Fig. 5H). These findings indicate that NFt1 is crucial for inducing lysosomal cell death in HCC cells.

3.6. Notoginsenoside Ft1 enhances TFEB transactivity regulating the lysosomal cell death

Given that genes related to lysosomal traits have previously been shown to be associated with transcription factor EB (TFEB), a central transcription factor [22], we investigated the interactions between *TFEB* and lysosomal cell death-related genes. Our findings revealed that a significant proportion of lysosome-associated genes (48.6 %; 34/70) interacted with TFEB. Additionally, lysosomal cell death-related genes, such as *TPP1*, *CTSB*, *CTSD*, *LAMP1*, and *LAMP2*, were confirmed to interact with *TFEB* (Fig. 6A). We also observed that TFEB binds to the promoter motifs of these genes (-2000 to +1 from the transcription start site), which contain core 5'-GTCACGTGAC-3' elements (Fig. 6B and C) [23,24]. However, NFt1 treatment did not elevate *TFEB* gene expression, but increased the expression of key regulatory molecules, *TSC1* and *TSC2*, in NFt1-treated cells ($P < 0.05$, Fig. 6D). The mTOR pathway is associated with TFEB transactivation and is regulated by TSC1 and TSC2 [25,26]. Using GSEA, we observed that NFt1-treated cells exhibited a decrease in mTOR-related gene signatures compared to untreated cells (Fig. 6E), which correlated with reduced phosphorylation of PI3K, AKT, mTOR, and the downstream effector p70S6K (Fig. 6F and Fig. S7). Additionally, NFt1 treatment led to a significant decrease in TFEB phosphorylation at Ser211 (Fig. 6G), which is linked to its translocation to the nucleus [27]. As expected, TFEB showed a marked increase in nuclear localization compared with in that untreated cells (Fig. 6H). Next, we constructed a 4xTFEB-binding motif reporter to analyze transactivation (Fig. S8) and demonstrated that NFt1 treatment significantly enhanced the activation of the 4xTFEB-binding promoter compared to untreated cells (Fig. 6I). Furthermore, we investigated the decrease in the phosphorylation of TFEB at Ser211 using xenograft mouse tissues from various treatment groups. NFt1-treated mice exhibited reduced phosphorylation of TFEB relative to the mock group (Fig. 6J). Collectively, our findings indicate that NFt1 treatment is instrumental in triggering lysosomal cell death through the activation of TFEB in HCC cells.

4. Discussion

We evaluated the anticancer properties of notoginsenoside Ft1 (NFt1) in hepatocellular carcinoma (HCC) and investigated the underlying molecular mechanisms that contribute to its therapeutic potential. Our results demonstrated that NFt1 significantly inhibits HCC cell proliferation and induces apoptosis *in vitro*. Specifically, NFt1 treatment resulted in a marked increase in apoptotic markers, such as PARP, caspase-8, caspase-9, and caspase-3, in HCC cell lines. However, the non-cancerous hepatic cell line THLE-2 was not affected by NFt1 treatment. This finding highlights the potential safety and specificity of NFt1 as a therapeutic agent for HCC. Additionally, NFt1 effectively suppressed tumor colony formation *in vitro* and significantly diminished tumor size in HepG2 xenograft model. These results underscore the therapeutic efficacy of NFt1 and suggest its utility as a promising agent for HCC treatment.

One major finding of this study is that NFt1 inhibits the MAPK signaling pathway, a critical regulator involved in HCC progression [28]. Transcriptomic analysis demonstrated a significant downregulation of MAPK-related oncogenes, including *FOS*, *JUND*, *NRAS*, and *KRAS*, in NFt1-treated cells. Consistently, protein analysis revealed a dose-dependent reduction in the expression of KRAS, c-Fos, and JUND, along with decreased phosphorylation of ERK1/2 and ELK-1. Interestingly, the phosphorylation of c-Jun was increased following NFt1 treatment, suggesting that the suppression of AP-1 transactivation by NFt1 is independent of c-Jun phosphorylation and is more closely associated with the downregulation of other AP-1 subunits such as c-Fos and JUND. Indeed, the regulation of AP-1 activity was induced by multiple mechanisms involving c-Fos and members of the Jun family, such as JUND and c-Jun [29]. Suppression of the MAPK pathway was accompanied by reduced AP-1 transactivation, indicating that NFt1 effectively targets this oncogenic signaling cascade. Notably, these effects were observed both *in vitro* and *in vivo*, with a significant reduction in MAPK-related proteins in NFt1-treated xenograft tissues. Given the significant involvement of the MAPK pathway in HCC pathogenesis and therapy resistance, these findings underscore the therapeutic relevance of NFt1 in targeting this pathway. Another major finding is the ability of NFt1 to induce lysosomal cell death, a relatively underexplored but promising therapeutic strategy for overcoming resistance in HCC. RNA-seq analysis revealed significant upregulation of lysosome-associated genes, including *CTSB*, *CTSD*, *LAMP1*, *LAMP2*, and *TPP1*, in NFt1-treated cells. Correspondingly, cathepsin B and D activity was significantly elevated in NFt1-treated cells and xenograft tissues, suggesting enhanced lysosomal function. Evidence for lysosomal cell death was strengthened by the elevated levels of LC3B-II and p62, markers of autophagosome formation and lysosomal degradation, respectively [30]. These findings highlight the dual role of NFt1 in promoting both apoptotic and lysosomal-mediated cell death, providing a complementary mechanism to conventional therapies.

TFEB, a key mediator of lysosomal biogenesis and autophagy, emerged as a pivotal regulator of NFt1-induced lysosomal cell death. NFt1 treatment enhanced TFEB nuclear translocation by reducing its phosphorylation at Ser211 [24], a modification that typically inhibits TFEB activity under basal conditions. This activation was associated with PI3K/AKT/mTOR cascade suppression, a well-established regulator of TFEB activation. NFt1 treatment decreased the PI3K, AKT, mTOR, and the downstream effector p70S6K phosphorylation, while

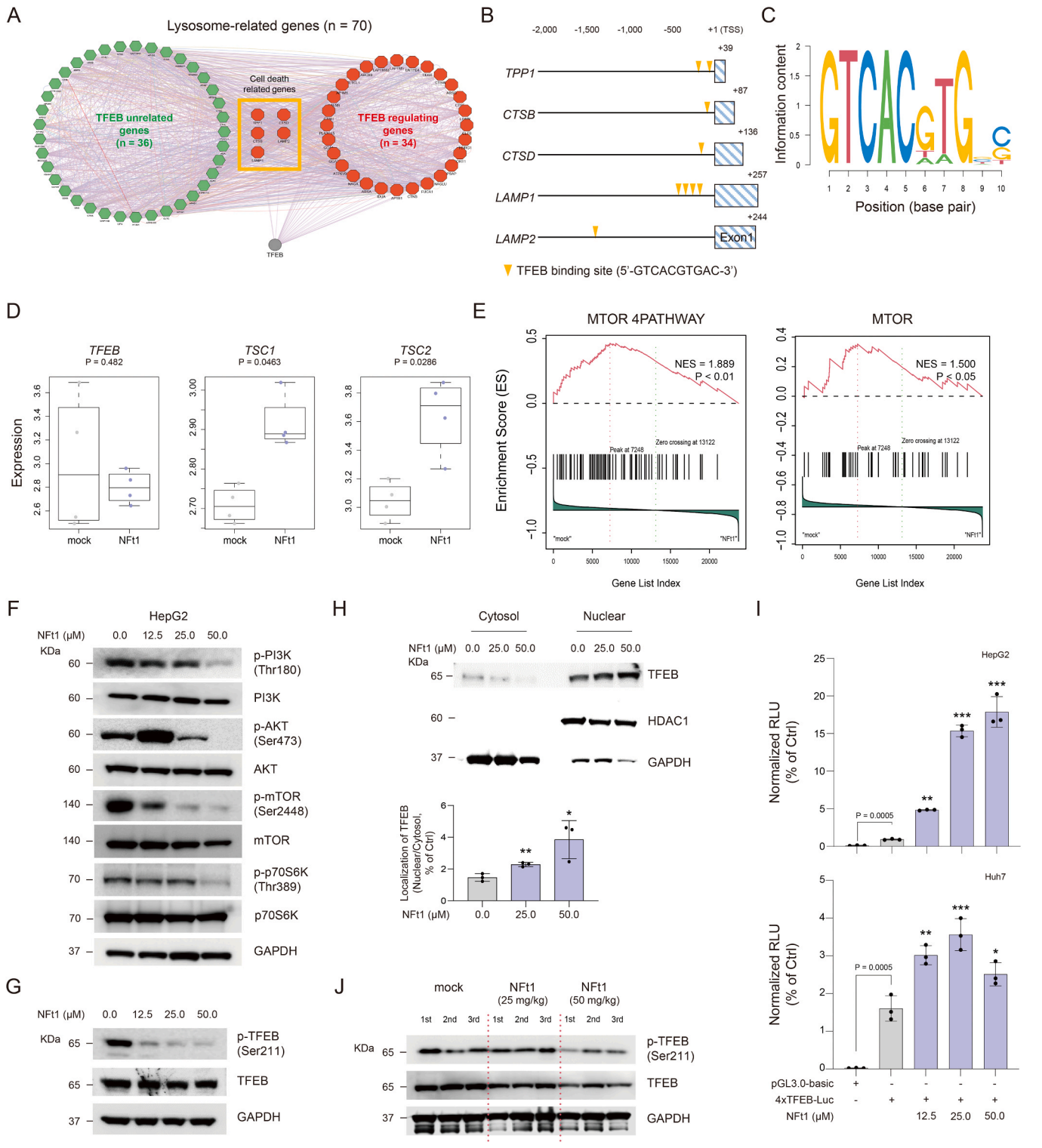

Fig. 6. Notoginsenoside Ft1 enhances TFEB transactivity regulating the lysosomal cell death. (A) A genetic network of lysosome-related genes ($n = 70$) was constructed in Cytoscape (version 3.9.1) using GeneMANIA, displaying various interaction types: physical (*pink*), co-localization (*purple*), genetic (*sky blue*), pathways (*green*), and predicted (*orange*). TFEB and lysosome-related cell death genes ($n = 5$) are highlighted. (B, C) The TFEB binding motif (5'-GTCACGTGAC-3') was identified on *TPP1*, *CTSB*, *CTSD*, *LAMP1*, and *LAMP2* using AliBaba2.1. Binding motifs (ten base pairs each) are shown. (D) The boxplots show the expression of lysosomal cell death-related genes, including *TFEB*, *TSC1*, and *TSC2*. (E) GSEA results show the enrichment of MTOR-related signatures (KEGG and REAC). (F) Western blot analysis of phospo-PI3K, PI3K, phospho-AKT, AKT, phospho-mTOR, mTOR, phospho-p70S6K, and p70S6K in HepG2 cells treated with NFt1 for 12 h. (G) Western blot analysis of phospo-TFEB and TFEB in HepG2 cells treated with NFt1 for 12 h. (H) TFEB translocation from the cytosol to the nucleus was visualized in treated cells, with GAPDH and HDAC1 serving as cytoplasmic and nuclear markers, respectively. (I) The barplot shows 4x TFEB transactivation in HepG2 and Huh7 cells following 24 h of NFt1 treatment, with significant *P*-value (*vs.* Ctrl; 2 line, $^{**}P < 0.01$ and $^{***}P < 0.001$). (J) Western blot analysis of phospho-TFEB and TFEB in HepG2 xenograft tissue untreated and treated with NFt1 (25 and 50 mg/kg).

increasing TSC1 and TSC2 levels, which are key negative regulators of mTORC1 [31,32]. The activation of TFEB was further confirmed by increased transactivity in a 4xTFEB-binding motif reporter assay and the upregulation of TFEB target genes, including lysosomal cell death markers such as *CTSB*, *CTSD*, *LAMP1*, and *LAMP2*. Collectively, these findings establish a novel mechanistic link between NFt1, PI3K/AKT/mTOR inhibition, and TFEB activation, highlighting the therapeutic potential of NFt1 in modulating lysosomal-mediated cell death pathway in HCC.

5. Conclusion

The findings of this study offer compelling evidence supporting the therapeutic potential of NFt1 in HCC. By simultaneously targeting multiple pathways, including MAPK signaling and PI3K/AKT/mTOR, and inducing lysosomal-mediated cell death, NFt1 offers a multifaceted strategy to overcoming the challenges of therapy resistance and tumor heterogeneity in HCC. Furthermore, the selective activity of NFt1 toward cancer cells, with minimal effects on normal hepatic cells, highlights its safety and specificity as a promising therapeutic agent.

Funding

This study was supported by multiple funding sources, including the institutional program of the Korea Institute of Science and Technology (KIST) under grant numbers 2E33521, as well as the National Research Foundation of Korea (NRF) under the government's MSIT funding (NRF-2022R1A6A3A01086490). Finally, the data were deposited in the KIST Dashboard.

CRediT authorship contribution statement

Youngsic Jeon: Writing – original draft, Visualization, Investigation, Formal analysis. **Young-Joo Kim:** Writing – review & editing, Writing – original draft, Supervision, Conceptualization. **Taejung Kim:** Writing – original draft, Supervision. **Dong-Young Woo:** Visualization, Investigation. **Ki Sung Kang:** Investigation. **Jun Yeon Park:** Investigation. **Su-Nam Kim:** Investigation. **Young Nyun Park:** Investigation, Conceptualization. **Taek Chung:** Visualization, Investigation. **Hyukjoon Kwon:** Visualization, Investigation.

Declaration of Competing Interest

The authors declare that they have no known competing financial interests or personal relationships that could have appeared to influence the work reported in this paper.

Appendix A. Supporting information

Supplementary data associated with this article can be found in the online version at doi:10.1016/j.biopha.2025.118181.

Data availability

Data will be made available on request.

References

[1] M. Ducreux, G.K. Abou-Alfa, T. Bekaii-Saab, J. Berlin, A. Cervantes, T. de Baere, C. Eng, P. Galle, S. Gill, T. Gruenberger, K. Haustermans, A. Lamarca, P. Laurent-Puig, J.M. Llovet, F. Lordick, T. Macarulla, D. Mukherji, K. Muro, R. Obermannova, J.M. O'Connor, E.M. O'Reilly, P. Osterlund, P. Philip, G. Prager, E. Ruiz-Garcia, B. Sangro, T. Seufferlein, J. Tabernero, C. Verslype, H. Wasan, E. Van Cutsem, The management of hepatocellular carcinoma. Current expert opinion and recommendations derived from the 24th ESMO/World Congress on Gastrointestinal Cancer, Barcelona, 2022, ESMO Open 8 (3) (2023) 101567.

[2] S. Qiu, J. Cai, Z. Yang, X. He, Z. Xing, J. Zu, E. Xie, L. Henry, C.R. Chong, E. M. John, R. Cheung, F. Ji, M.H. Nguyen, Trends in hepatocellular carcinoma mortality rates in the US and Projections Through 2040, JAMA Netw. Open 7 (11) (2024) e2445525.

[3] A. Huang, X.R. Yang, W.Y. Chung, A.R. Dennison, J. Zhou, Targeted therapy for hepatocellular carcinoma, Signal Transduct. Target Ther. 5 (1) (2020) 146.

[4] Y. Feng, Y. Li, F. Ma, E. Wu, Z. Cheng, S. Zhou, Z. Wang, L. Yang, X. Sun, J. Zhang, Notoginsenoside Ft1 inhibits colorectal cancer growth by increasing CD8(+) T cell proportion in tumor-bearing mice through the USP9X signaling pathway, Chin. J. Nat. Med 22 (4) (2024) 329–340.

[5] K. Shen, S.W. Leung, L. Ji, Y. Huang, M. Hou, A. Xu, Z. Wang, P.M. Vanhoutte, Notoginsenoside Ft1 activates both glucocorticoid and estrogen receptors to induce endothelium-dependent, nitric oxide-mediated relaxations in rat mesenteric arteries, Biochem Pharm. 88 (1) (2014) 66–74.

[6] E. Zhang, B. Gao, L. Yang, X. Wu, Z. Wang, Notoginsenoside Ft1 promotes fibroblast proliferation via PI3K/Akt/mTOR signaling pathway and benefits wound healing in genetically diabetic mice, J. Pharm. Exp. Ther. 356 (2) (2016) 324–332.

[7] N. Grabinski, F. Ewald, B.T. Hofmann, K. Staufer, U. Schumacher, B. Nashan, M. Jucker, Combined targeting of AKT and mTOR synergistically inhibits proliferation of hepatocellular carcinoma cells, Mol. Cancer 11 (2012) 85.

[8] S.U. Khan, A.S. Pathania, A. Wani, K. Fatima, M.J. Mintoo, B. Hamza, M.A. Paddar, W. Bhumika, L.K. Anand, M.S. Maqbool, S.A. Mir, J. Kour, V. Venkateswarlu, D. M. Mondhe, S.D. Sawant, F. Malik, Author Correction: activation of lysosomal mediated cell death in the course of autophagy by mTORC1 inhibitor, Sci. Rep. 12 (1) (2022) 8772.

[9] B. Zhitomirsky, A. Yunaev, R. Kreiserman, A. Kaplan, M. Stark, Y.G. Assaraf, Lysosomotropic drugs activate TFEB via lysosomal membrane fluidization and consequent inhibition of mTORC1 activity, Cell Death Dis. 9 (12) (2018) 1191.

[10] Z. Cui, G. Napolitano, M.E.G. de Araujo, A. Esposito, J. Monfregola, L.A. Huber, A. Ballabio, J.H. Hurley, Structure of the lysosomal mTORC1-TFEB-Rag-Ragulator megacomplex, Nature 614 (7948) (2023) 572–579.

[11] M. Palmieri, R. Pal, H.R. Nelvagal, P. Lotfi, G.R. Stinnett, M.L. Seymour, A. Chaudhury, L. Bajaj, V.V. Bondar, L. Bremner, U. Saleem, D.Y. Tse, D. Sanagasetti, S.M. Wu, J.R. Neilson, F.A. Pereira, R.G. Pautler, G.G. Rodney, J. D. Cooper, M. Sardiello, mTORC1-independent TFEB activation via Akt inhibition promotes cellular clearance in neurodegenerative storage diseases, Nat. Commun. 8 (2017) 14338.

[12] N. Raben, R. Puertollano, TFEB and TFE3: linking lysosomes to cellular adaptation to stress, Annu Rev. Cell Dev. Biol. 32 (2016) 255–278.

[13] C.G. Towers, A. Thorburn, Targeting the lysosome for cancer therapy, Cancer Discov. 7 (11) (2017) 1218–1220.

[14] Y. Jeon, J. Kim, H. Kwon, Y.J. Yeon, T. Kim, J. Ham, Y.J. Kim, Cannabiorcol as a novel inhibitor of the p38/MSK-1/NF-kappaB signaling pathway, reducing matrix metalloproteinases in osteoarthritis, Phytomedicine 135 (2024) 156141.

[15] C. Trapnell, A. Roberts, L. Goff, G. Pertea, D. Kim, D.R. Kelley, H. Pimentel, S. L. Salzberg, J.L. Rinn, L. Pachter, Differential gene and transcript expression analysis of RNA-seq experiments with TopHat and Cufflinks, Nat. Protoc. 7 (3) (2012) 562–578.

[16] A. Subramanian, P. Tamayo, V.K. Mootha, S. Mukherjee, B.L. Ebert, M.A. Gillette, A. Paulovich, S.L. Pomeroy, T.R. Golub, E.S. Lander, J.P. Mesirov, Gene set enrichment analysis: a knowledge-based approach for interpreting genome-wide expression profiles, Proc. Natl. Acad. Sci. USA 102 (43) (2005) 15545–15550.

[17] Y. Liu, J. Sun, M. Zhao, ONGene: a literature-based database for human oncogenes, J. Genet Genom. 44 (2) (2017) 119–121.

[18] M. Zhao, P. Kim, R. Mitra, J. Zhao, Z. Zhao, TSGene 2.0: an updated literature-based knowledgebase for tumor suppressor genes, Nucleic Acids Res 44 (D1) (2016) D1023–D1031.

[19] P.A. Farazi, R.A. DePinho, Hepatocellular carcinoma pathogenesis: from genes to environment, Nat. Rev. Cancer 6 (9) (2006) 674–687.

[20] T. Kirkegaard, M. Jaattela, Lysosomal involvement in cell death and cancer, Biochim Biophys. Acta 1793 (4) (2009) 746–754.

[21] N. Fehrenbacher, L. Bastholm, T. Kirkegaard-Sorensen, B. Rafn, T. Bottzauw, C. Nielsen, E. Weber, S. Shirasawa, T. Kallunki, M. Jaattela, Sensitization to the lysosomal cell death pathway by oncogene-induced down-regulation of lysosome-associated membrane proteins 1 and 2, Cancer Res 68 (16) (2008) 6623–6633.

[22] C. Settembre, C. Di Malta, V.A. Polito, M.Garcia Arencibia, F. Vetrini, S. Erdin, S. U. Erdin, T. Huynh, D. Medina, P. Colella, M. Sardiello, D.C. Rubinsztein, A. Ballabio, TFEB links autophagy to lysosomal biogenesis, Science 332 (6036) (2011) 1429–1433.

[23] M. Sardiello, M. Palmieri, A. di Ronza, D.L. Medina, M. Valenza, V.A. Gennarino, C. Di Malta, F. Donaudy, V. Embrione, R.S. Polishchuk, S. Banfi, G. Parenti, E. Cattaneo, A. Ballabio, A gene network regulating lysosomal biogenesis and function, Science 325 (5939) (2009) 473–477.

[24] W. Zhang, X. Li, S. Wang, Y. Chen, H. Liu, Regulation of TFEB activity and its potential as a therapeutic target against kidney diseases, Cell Death Discov. 6 (2020) 32.

[25] C. Luo, W.R. Ye, W. Shi, P. Yin, C. Chen, Y.B. He, M.F. Chen, X.B. Zu, Y. Cai, Perfect match: mTOR inhibitors and tuberous sclerosis complex, Orphanet J. Rare Dis. 17 (1) (2022) 106.

[26] M. Taneike, K. Nishida, S. Omiya, E. Zarrinpashneh, T. Misaka, R. Kitazume-Taneike, R. Austin, M. Takaoka, O. Yamaguchi, M.J. Gambello, A.M. Shah, K. Otsu, mTOR Hyperactivation by Ablation of Tuberous Sclerosis Complex 2 in the Mouse Heart Induces Cardiac Dysfunction with the Increased Number of Small Mitochondria Mediated through the Down-Regulation of Autophagy, PLoS One 11 (3) (2016) e0152628.

[27] J.A. Martina, Y. Chen, M. Gucek, R. Puertollano, MTORC1 functions as a transcriptional regulator of autophagy by preventing nuclear transport of TFEB, Autophagy 8 (6) (2012) 903–914.

[28] S. Whittaker, R. Marais, A.X. Zhu, The role of signaling pathways in the development and treatment of hepatocellular carcinoma, Oncogene 29 (36) (2010) 4989–5005.
[29] H. Gille, T. Strahl, P.E. Shaw, Activation of ternary complex factor Elk-1 by stress-activated protein kinases, Curr. Biol. 5 (10) (1995) 1191–1200.
[30] E.R. Gallagher, E.L.F. Holzbaur, The selective autophagy adaptor p62/SQSTM1 forms phase condensates regulated by HSP27 that facilitate the clearance of damaged lysosomes via lysophagy, Cell Rep. 42 (2) (2023) 112037.
[31] M. Lai, W. Zou, Z. Han, L. Zhou, Z. Qiu, J. Chen, S. Zhang, P. Lai, K. Li, Y. Zhang, L. Liang, Y. Jiang, Z. Zou, X. Bai, Tsc1 regulates tight junction independent of mTORC1, Proc. Natl. Acad. Sci. USA 118 (30) (2021).
[32] C.P. Lin, J.J.H. Traets, D.W. Vredevoogd, N.L. Visser, D.S. Peeper, TSC2 regulates tumor susceptibility to TRAIL-mediated T-cell killing by orchestrating mTOR signaling, EMBO J. 42 (5) (2023) e111614.